**Taylor & Francis**
Taylor & Francis Group

∂ OPEN ACCESS | Check for updates

# The impact of employing a magnetic field as well as $Fe_3O_4$ nanoparticles on the performance of phase change materials

Mohammad Zandie[a], Amirhossein Moghaddas[b], Alireza Kazemi[c], Mohammad Ahmadi[a], Hadi Nikbin Feshkache[d], Mohammad Hossein Ahmadi [ID][e] and Mohsen Sharifpur[f,g]

[a]Department of Petroleum Engineering, School of Petroleum Engineering, Amirkabir University of Technology, Tehran, Iran; [b]Department of Mechanical Engineering, Islamic Azad University, Science and Research Branch, Tehran, Iran; [c]Department of Petroleum and Chemical Engineering, Sultan Qaboos University, Muscat, Oman; [d]Department of Chemical and Petroleum Engineering, Sharif University of Technology, Tehran, Iran; [e]Faculty of Mechanical Engineering, Shahrood University of Technology, Shahrood, Iran; [f]Clean Energy Research Group, Department of Mechanical and Aeronautical Engineering, Engineering III, University of Pretoria, Pretoria, South Africa; [g]Department of Medical Research, China Medical University Hospital, China Medical University, Taichung, Taiwan

**ABSTRACT**

In this study a 2D cubic chamber model filled with paraffin is analyzed with and without the inclusion of magnetic $Fe_3O_4$ nanoparticles at concentrations of 0.5, 1, 1.5 and 2 wt%, and an external magnetic field of intensities 0.005, 0.01, 0.015 and 0.02 T. It is ascertained that adding magnetic nanoparticles leads the horizontal temperature gradient to be reduced owing to increments in thermal conductivity. Additionally, this feature is found to be accelerated by applying an external magnetic field, which shapes highly conductive cluster formations of nanoparticles. However, since the increase in nanoparticle concentration and magnetic intensity increases the composite viscosity, there is an optimum configuration while applying both schemes. As such, the addition of 1 wt% nanoparticles provides the best results, as the melting time is reduced up to 25% compared to pure paraffin. Meanwhile, the melting time of a 1 wt% nanoparticle-containing phase change material (PCM) in the presence of an external magnetic field is improved up to 24% compared to the case with no external magnetic field. Also, the heat transfer coefficient of a 1 wt% nanoparticle-containing PCM both with and without an external magnetic field is also staggeringly enhanced compared to pure paraffin. Good correspondence with experimental data was achieved.

## Introduction

To date, the problematic drawbacks associated with fossil fuel utilization on the one hand and the critical need for energy supplies on the other have emphasized the necessity of finding proper alternatives to fossil fuels more than ever. To this end, renewable energies have been introduced worldwide to serve this purpose; however, the main limitation associated with these resources is the lack of permanent availability, which leads them to be coupled with energy storage systems. Therefore, the provision of appropriate means for storing this energy is considered to be of paramount significance (Band et al., 2021; Khorampoor et al., 2020).

Thermal energy storage (TES) is carried out mainly by changing a material's inherent energy, which can be categorized as chemical, latent or sensible heat storage, or a combination of all the above (Ahmed et al., 2019).

Given the ability of latent heat storage systems to store energy at a constant temperature, in addition to their high energy storage capacities, noticeable attention has been received in this field (Ghoghaei et al., 2020; Kyriaki et al., 2018). Throughout the latent heat storage process, thermal energy is either absorbed or released by phase change materials (PCMs) when the phase change process takes place. PCMs are currently being applied in various industrial fields such as battery thermal management (Chiew et al., 2019; Ghadbeigi et al., 2018; Huang et al., 2019; Rao et al., 2013), electronic cooling systems (Mohammadi et al., 2021; Yoon et al., 2018) and building envelopes (Chiew et al., 2018; Romanchenko et al., 2018).

Despite the aforementioned beneficial aspects of PCMs, their applicability is limited by low thermal conductivity, which ultimately leads to problems with the rates of charge and discharge. This downside is of more

---

concern in cases of high heat transfer efficiency needs. To date, there have been major attempts to address this issue by using particles with high thermal conductivity combined with PCMs (Kibria et al., 2015), metal foams and fins (Dhaidan & Khodadadi, 2017) and intermediate fluids (Hosseininaveh et al., 2021; Martin et al., 2010; Ramazani et al., 2020). Among the proposed solutions to improve the PCMs' thermal conductivity, the dispersion of metal particles has gained much interest recently.

The superior features of newly introduced PCMs equipped with dispersed metals have proven to be promising regarding their storage capacity and heat transfer compared to traditional types of PCM (Liu et al., 2016; Selimefendigil & Öztop, 2020). Nourani et al. (2016) proposed an $Al_2O_3$ particles-enhanced paraffin wax. They revealed that the thermal conductivity and melting rate were improved by 31% and 27%, respectively, for the optimum nanoparticle concentration. They also stated that a constant increase in the nanoparticle mass fraction not only did not contribute to the optimum state, but also brought about negative impacts. The main reason for such an occurrence was attributed to the commensurate rise of nanocomposite viscosity with the rise in nanoparticle mass fraction. A dispersion of ZnO nanoparticles in ethylene glycol was investigated by Li et al. (2015). Their results showed a significant improvement in the thermal conductivity of the employed composite employed. Sharma et al. (2016) conducted similar research for $TiO_2$ nanoparticles. A significant improvement was achieved for the thermal conductivity of the proposed composite by up to 80%.

Furthermore, employing nanoparticles with well-suited magnetic properties is among the most newly introduced techniques in controlling heat exchange efficiency (Baghban et al., 2019; Sathiyamoorthy & Chamkha, 2010). As such, in a study conducted by Sundar et al. (2013) it was found that magnetic nanoparticles can improve the thermal conductivity of the fluid by up to 40%. Hence, nanocomposites with high thermal conductivity and magnetic properties can act as a better substitute to enhance the phase changing features of PCMs, rather than simply improving the heat transfer via conduction. This is because the storage process and the heat transfer rate are found to be managed precisely through a proper magnetic field configuration (Bahiraei & Hangi, 2015; Qi et al., 2021; Selimefendigil & Chamkha, 2016; Sheikholeslami & Rokni, 2017). Park et al. (2014) investigated the characterization of magnetic $Fe_3O_4$ nanoparticles combined with PCM nanocapsules under external magnetic field condition. They indicated that the thermal conductivity of the incorporated nanocapsules increased significantly with an increase in the nanoparticle concentration as well as with an increase in the intensity of the external magnetic field. Their model was also feasible to use for developing smart PCM materials with a diverse range of industrial and biomedical applications. A similar study was conducted by Lashgari et al. (2018) on an experimental scale, where the thermal conductivity of a nanoparticle-enhanced PCM microcapsule employed was found to be linearly proportional to an increase in nanoparticle content when a magnetic field was applied.

Sheikholeslami and Mahian (2019) explored the enhancement of PCM solidification in the presence of inorganic nanoparticles and an external magnetic field. They revealed that the solidification time could be reduced by up to 14% in the best scenario. In interesting research performed by Ghachem et al. (2021), the effects of a rotating conic surface and a magnetic field on the phase change dynamics were numerically examined for a PCM-filled cylindrical reactor. Their results revealed that the coupled integration of the rotating surface in conjunction with the magnetic field resulted in an enhancement in the phase change process dynamics. They also concluded that the rotating surface reduced the full phase transition time by up to 98% in the best case study. Selimefendigil et al. (2019) analyzed the natural convection of magnetohydrodynamic (MHD) flow in a 2D cavity filled with CuO–water nanofluid and a PCM. Their study revealed that the strength and the inclination of the magnetic field, and the thermal and electrical conductivity properties of the nanofluid, had substantial improving impacts on the fluid flow and the heat transfer of the nanofluid.

In this research, a novel scheme is proposed to improve the heat transfer and phase change properties of PCMs through the simultaneous calibration of the applied magnetic field intensity and the magnetic nanoparticle concentration using computational fluid dynamics (CFD) software. The configuration and system setup are in accordance with the experimental work of Sadegh et al. (2020). It must be noted that, throughout their work, only a limited range of nanoparticles concentration and magnetic field intensity was tested. Nonetheless, in this study the respective range is meticulously diversified to examine the results of their work accurately. Moreover, the outcomes of this investigation have been extensively analyzed from various standpoints including the flow and thermal behavior of the composite under applied strategies, in addition to providing a more distinct visualization of the melting-related phenomena. As such, a 2D rectangular shaped chamber model is designed to inspect the contributions of declared techniques in terms of temperature field, melting process and melting time. To this end, four magnetic nanoparticle concentrations of 0.5, 1, 1.5 and 2 wt% with and without an external magnetic field with intensities of 0.005,

0.01, 0.015 and 0.02 T are applied. Also, in most previous investigations, the properties of nanocomposites were assumed to be the average of the nanoparticles and the base PCM, which could impose unfavorable inaccuracies throughout the simulations. In contrast, the materials employed in this study are defined separately to eliminate the necessity of approximating the nanocomposite thermal properties and to improve the accuracy and validity of the results.

## Numerical methodology

### Physical model

As shown in Figure 1, a 2D rectangular shape chamber of dimensions 70 × 48 mm is considered fully filled with pure paraffin in its solid phase state and ambient temperature at the commencement of simulations. The reason behind the selection of the abovementioned dimension is that in this study it has been attempted to regenerate the experimental work of Sadegh et al. (2020), in which the findings of their study are meant to be investigated numerically in a detailed manner to visualize the hypothesis made (Sadegh et al., 2020). On the other hand, it is also tried to explore the applied strategies, namely the integration of magnetic nanoparticles and the external magnetic field, with additional case studies as declared earlier. Thus, to provide a comparative analysis relevant to the work of Sadegh et al. (2020), all the utilized configurations are given precisely analogous.
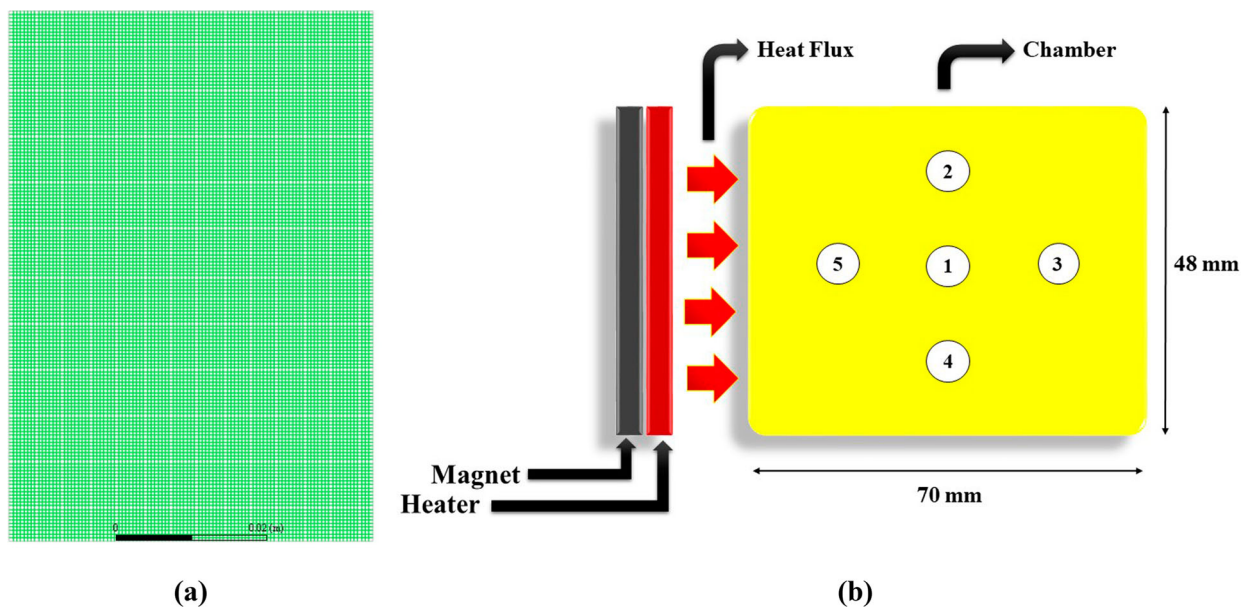
**Table 1.** Thermal specifications of applied materials. [a]

| | Melting point (°C) | Latent heat (kJ/kg) | Density at 80 °C (kg/m$^3$) | Thermal conductivity at 70 °C (W/mK) | Viscosity at 100 °C (cSt) |
|---|---|---|---|---|---|
| Paraffin | 65 | 142 | 760 | 0.23 | 7 |
| Magnetite | 1870 | – | 7874 | 9.7 | – |

[a]The values are reported for a specific condition, but a range of properties under various conditions are provided to the system for the simulation setup.

### Thermal properties of phase change material composites

The thermal properties of paraffin and magnetite nanoparticles are given in Table 1. The thermal properties of each individual phase are given for the system under various conditions, since the composites' thermal properties vary with fluctuations in the boundary conditions. Moreover, although there have been similar numerical studies, such as the work conducted by Hu et al. (2020), however, throughout their investigations, the properties of the nanocomposites have not been considered separately and the features studied have been assumed to be the properties of the total mixture. Nevertheless, in this research the properties of each phase (paraffin and magnetite nanoparticles) are defined separately, which can increase the accuracy of the simulations, particularly when a magnetic field is applied.

To this end, two distinct files in the material section of Fluent® containing respective properties for PCM and nanoparticles have been defined in the software. Then,



**Figure 1.** Schematic of: (a) the mesh structure; and (b) the system setup.

by using the patch dialog box in the initialization module of Fluent, the intended volume fraction, according to data reported by Sadegh et al. (2020), for nanoparticles are patched to the desired (interior) surface. The system will then automatically try a homogenous propagation of nanoparticles within the PCM phase, and it will assign separate cells to PCMs and nanoparticles accordingly (Fluent, 2019).

## Governing equations

In this study, the volume of fluid (VOF) method is employed to simulate the system. The left-hand side of the chamber is assumed to be the inlet, where a constant heat flux (equivalent to 6 W or approximately 1786 W/m$^2$) and an external magnetic field are applied, while the other three sides are assumed to be adiabatic (isolated) and impermeable. The Boussineq approximation is also utilized for the natural convection effect (Hu et al., 2020; Kumar & Krishna, 2017). The Lorenz force and Joule heating were ignored throughout the simulations since the composite does not have electrical conduction. The dimensionless equations associated with model simulations are listed as follows:

$$Pr = \frac{v}{\propto} \qquad (1)$$

$$Ra = \frac{g\beta(T_h - T_c)X^3}{v \propto} \qquad (2)$$

$$St = \frac{C_p(T_h - T_c)}{L} \qquad (3)$$

$$Fo = \frac{\propto t}{l^2} \qquad (4)$$

The formulation of the mass and heat transfer equations for the phase change process are also discussed below. It is important to note that the flow regime is determined to be laminar, and the fluid is incompressible (Luo et al., 2015). Moreover, given the variations in the composite thermal properties, the addition of the nanoparticle and materials fractions can lead the properties of the mixture to vary. But, since the properties of the materials are defined distinctly, once the percentage of the phase mass fraction (or volume fraction) is defined, the module will automatically measure the composite properties without manual intervention.

The continuity equation is as follows (Aghaei et al., 2021; Zandie et al., 2021):

$$\frac{\partial \rho}{\partial t} + \nabla . (\rho u) = 0 \qquad (5)$$

in which $\rho$ and $u$ stand for density and velocity vector, respectively. The momentum equation can be written as follows (Ghalandari et al., 2019):

$$\frac{\partial (\rho u)}{\partial t} + \nabla \cdot (\rho u u) = -\nabla p + \nabla \cdot (\mu \nabla u) + \rho n \qquad (6)$$

$$n = n_b + n_m \qquad (7)$$

in which $p$ and $\mu$ denote pressure and dynamic viscosity, respectively. Moreover, $n$ is defined as the exterior body force per unit mass, which is formulated as follows (Turner, 1979):

$$n_b = g\beta(T - T_{ref}) \qquad (8)$$

$$n_m = u_0 m_0 \nabla M \qquad (9)$$

in which $\beta, g, T$ and $T_{ref}$ are the thermal expansion, gravitational acceleration, temperature and reference temperature (ambient temperature), respectively. Furthermore, $u_0$, $m_0$ and $\nabla M$ are the vacuum permeability, nanoparticles bulk magnetism and magnetic intensity gradient, respectively. Also, the energy equation can be given as follows (Hu et al., 2020; Yang et al., 2020):

$$\frac{\partial (\rho c_p T)}{\partial t} + \nabla . (\rho c_p u T) = \nabla . (k \nabla T) + \dot{q} \qquad (10)$$

where $C_p$, $k$ and $\dot{q}$ are specific heat capacity, thermal conductivity and latent heat term, respectively. The latent heat term is formulated as follows (Hu et al., 2020):

$$\dot{q} = -\left[\frac{\partial (\rho u n H)}{\partial t} + \nabla . (\rho u u n H)\right] \qquad (11)$$

where $H$ indicates the total latent enthalpy throughout the phase change, which is defined as the change in temperature multiplied by the heat capacity. The liquid fraction is calculated as the change in enthalpy per latent heat, $\gamma = \Delta H/L$. It is worth mentioning that, in case of pure materials, the right-hand terms in the latent heat equation equal zero, and $\dot{q}$ can be represented as

$$\dot{q} = -\frac{\partial(\rho n H)}{\partial t} = -\frac{\partial(\rho L \gamma)}{\partial t} \qquad (12)$$

## Mesh independency analysis

Since a well-crafted mesh structure warrants the best analysis outcomes, reduces the necessity for extra time-consuming runs and more importantly improves the simulation prediction competency, it is then attempted to perform a mesh independency analysis (Karar et al., 2021; Zandie et al., 2021). In general, a mesh structure with high resolution requires the least size change from one cell to adjacent cells. Thus a smooth growth in size for meshing cells is of paramount importance in order to avoid poor computational results. As declared earlier, ANSYS$^{\circledR}$ Fluent 19.0 is used to conduct the tests, while
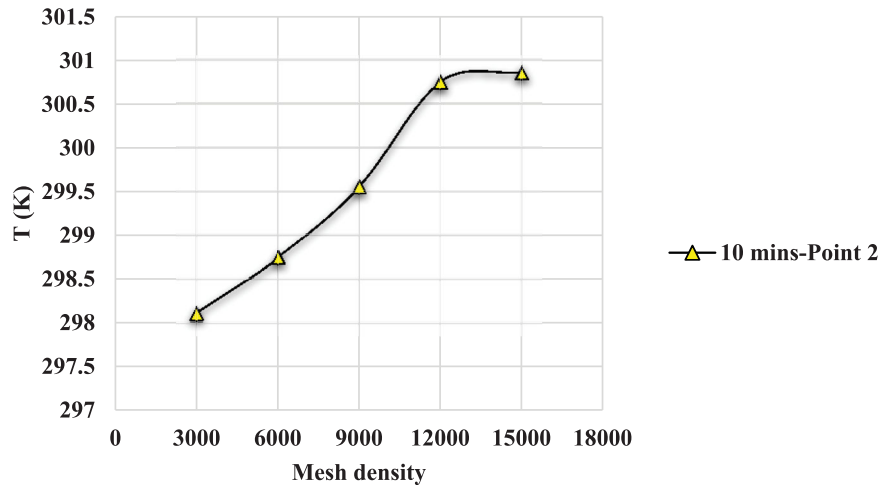
**Figure 2.** Temperature variation of pure paraffin melting at point 2 under different mesh densities.

the Integrated Computer Engineering and Manufacturing (ICEM) module is utilized to mesh the structure of the system. Five mesh densities of 3000, 6000, 9000, 12,000 and 15,000 were applied, and it was perceived that the density of 12,000 perfectly met the requirements of a high-quality mesh, and consequently, sizing the numerical results were not affected significantly. Also, since the structure of the chamber is rectangular, the quality of the mesh will be more likely to be high regardless of the meshing structure. Thus, the grid type was structured using a medium-mesh strategy in order to avoid unnecessary extra computational time.

Furthermore, as for the first layer thickness of the boundary layer grid, it must be noted that since all the four corners as well as all the cells are important for monitoring the melting process, the growth rate option has been fixed to one to homogenize the cell measurements. Thus, the first layer thickness is calculated as the length of the particular boundary layer according to the number of divisions, which in this case is 1 mm. A minimum orthogonal quality benchmark was also utilized to assess the suitability of the mesh sizes chosen. The retrieved mesh quality was very close to one (0.99), where values close to zero denote poor quality and values close to one illustrate high mesh quality. In addition, the absolute residual convergence criteria for continuity, velocity and energy have been fixed at $10^{-5}$, $10^{-5}$ and $10^{-6}$, respectively. As for the pressure–velocity coupling, the SIMPLE scheme has been employed. Three time steps of 0.01, 0.1 and 1 s were examined and the convergence criteria were found to be compromised in the case of 1 s. However, no sharp difference between 0.01 and 0. 1 s was noticed. Hence, a time step size of 0.1 s was used throughout the simulations. Additionally, a variable number of iterations (between 50 and 100) per time step has been used, as suggested by Kheirabadi and Groulx (2015). As such, at the beginning stage of the melting process, convergence was achieved faster (owing to the conduction form of heat transfer), while for the later stages, convergence required more iterations to meet the criteria.

It is worthy of note that the spatial discretization for pressure has been selected to be PRESTO, while second order upwind method was used for momentum and energy discretization. Another important constant that must be declared is the Courant number, which is defined as the time that the solution focuses on one cell of the mesh, or how long a particle stays in one cell. This value must be kept below one (ideally below 0.7) (Fluent, 2019; Rösler & Brüggemann, 2011), while in this study it has been fixed at 0.25 to ensure accurate simulation results. Figure 2 gives a schematic of the temperature variation for pure paraffin case point 2 (the location of assumed point is according to Figure 1) for various mesh densities and 10 min of flow time.

### Mushy zone constant

The mushy zone is defined as a semi-solid region present at the interface film between the melted and the unmelted section of PCMs (Kumar & Krishna, 2017). This region has been found to enormously affect the overall flow characteristics as well as the heat transfer throughout the melting and solidification processes (Marri & Balaji, 2022; Yang et al., 2020). Therefore, in this study, it also attempted to analyze the effects of different mushy zone constants ($A_{mush}$). To this end, three mushy zone constants, $A_{mush} = 10^3$, $10^5$ and $10^8$ kg/m$^3$s, for two time intervals of 24 and 60 min have been investigated and the results in terms of streamline function contours are illustrated in Figure 3. To begin with, the melting front inclination increases by the increase in the mushy zone constant value. Moreover, by increasing the time duration,
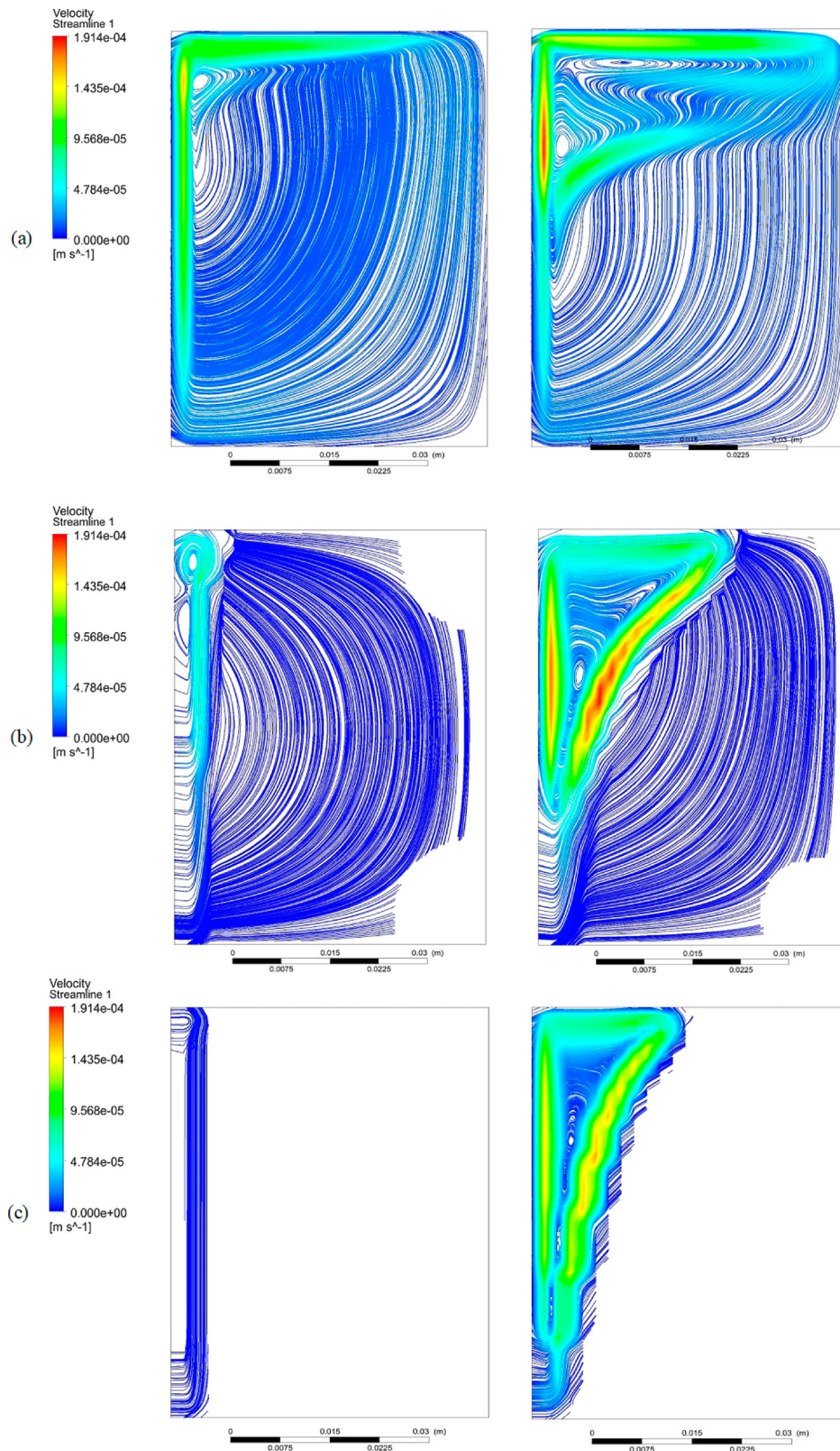
**Figure 3.** Streamline function contours for mushy zone constants of: (a) $10^3$; (b) $10^5$; and (c) $10^8$ kg/m$^3$ s.

more skew-shaped streamlines are noticed, which are due to the increase in the buoyancy effect and the dominance of convective currents throughout the upper sections compared to the lower section of the melted areas.

Furthermore, the increase in the value of the mushy zone constant would lead to a greater diffusion term, which consequently overpowers the convective term (Kumar & Krishna, 2017). On the other hand, with the
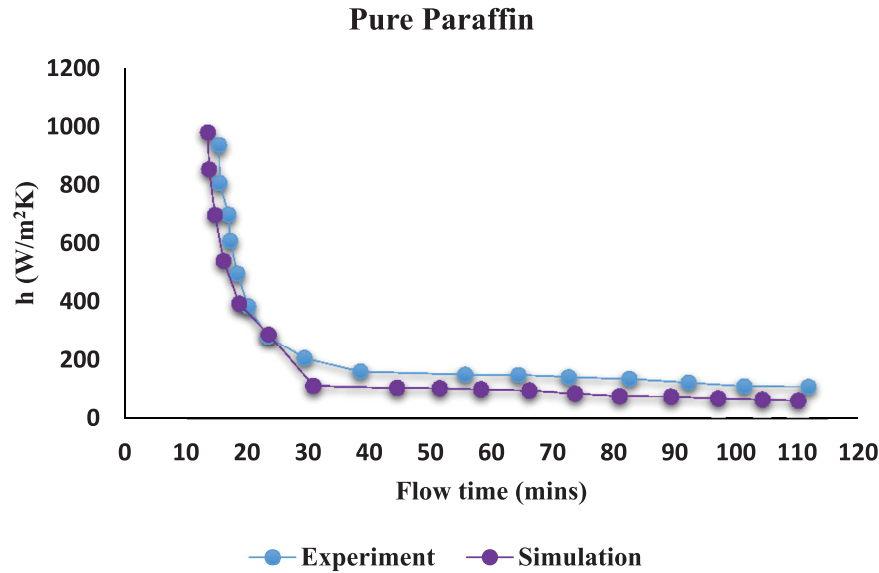
**Pure Paraffin**



**Figure 4.** Comparison of simulated and experimental heat transfer coefficients (Sadegh et al., 2020).

increase in the mushy zone constant, a decrease in heat transfer is expected to occur, which is attributed to the decrease in the convection strength. In summary, greater mushy zone values correspond to a more delayed phase change process since they cause heavier flow resistance (Yang et al., 2020). This event weakens the associated convective heat transfer within the mushy zone. It is worthy of note that, for higher mushy zone constants ($10^8$ kg/m$^3$s), heat transfer takes place by conduction, while for lower mushy zone values ($10^5$ kg/m$^3$s) both convection and conduction influence the heat transfer. This phenomenon is in line with previous investigations (Arıcı et al., 2017; Hameter & Walter, 2016; Kheirabadi & Groulx, 2015). The difference in heat transfer coefficients has been utilized as one of the criteria to find the optimum configuration of the mushy zone constant; as such, the measured heat transfer coefficient has been compared to that of experimental data and a mushy zone constant of $10^5$ kg/m$^3$s turned out to correspond the best with the experimental data. The results of the next stage (validation of the numerical model) are based on the optimum mushy zone constant. In addition, as can be observed in Figure 3, higher values of the mushy zone constant give sharper curvature along to the melting interface, and comparison with the figures given in the work of Sadegh et al. (2020) reveals that $A_{mush} = 10^5$ kg/m$^3$s corresponds much better with the experimental results.

### *Validation of the numerical model*

The authenticity of simulation results must also be verified to ensure the reliability of the approach. Given the inherent difficulties associated with experimental

investigations such as limited accessibility to precise capture of the temperature distribution and numerical measurements relevant to the liquid–solid interface area, the heat transfer coefficient ($h$) for the pure paraffin case study is benchmarked. The definition of this parameter is demonstrated in Heat transfer coefficient section. As shown in Figure 4, conducting a comparison between the outcomes of the experimental and numerical models reveals an acceptable correspondence between the simulations' predictions and the experimental data. As such, the highest error of 18% has been archived at a flow time of 30 min.

### Results and discussion

### *Phase change characteristics of different nanoparticle concentrations*

Figures 5 and 6 represent the melting process of pure paraffin and nanoparticle-enhanced composites with different mass fractions. As can be conceived, the solid phase tends to melt primarily from the side exposed to the heater (the left-hand side). At the commencement of melting, the melting profile is mainly parallel to the left axis, which is attributed to the low convective heat transfer. In fact, during this time, the main mode of heat transfer is conduction. As time passes, the liquid volume fraction increases with rising temperature, and as a result, the convection mode is strengthened, which causes the melting profile to be curved. This curvature in the melting profile is more observable in the upper sections of the chamber, which is due to the buoyancy force of the liquid phase (caused by the movement of the less-dense phase)
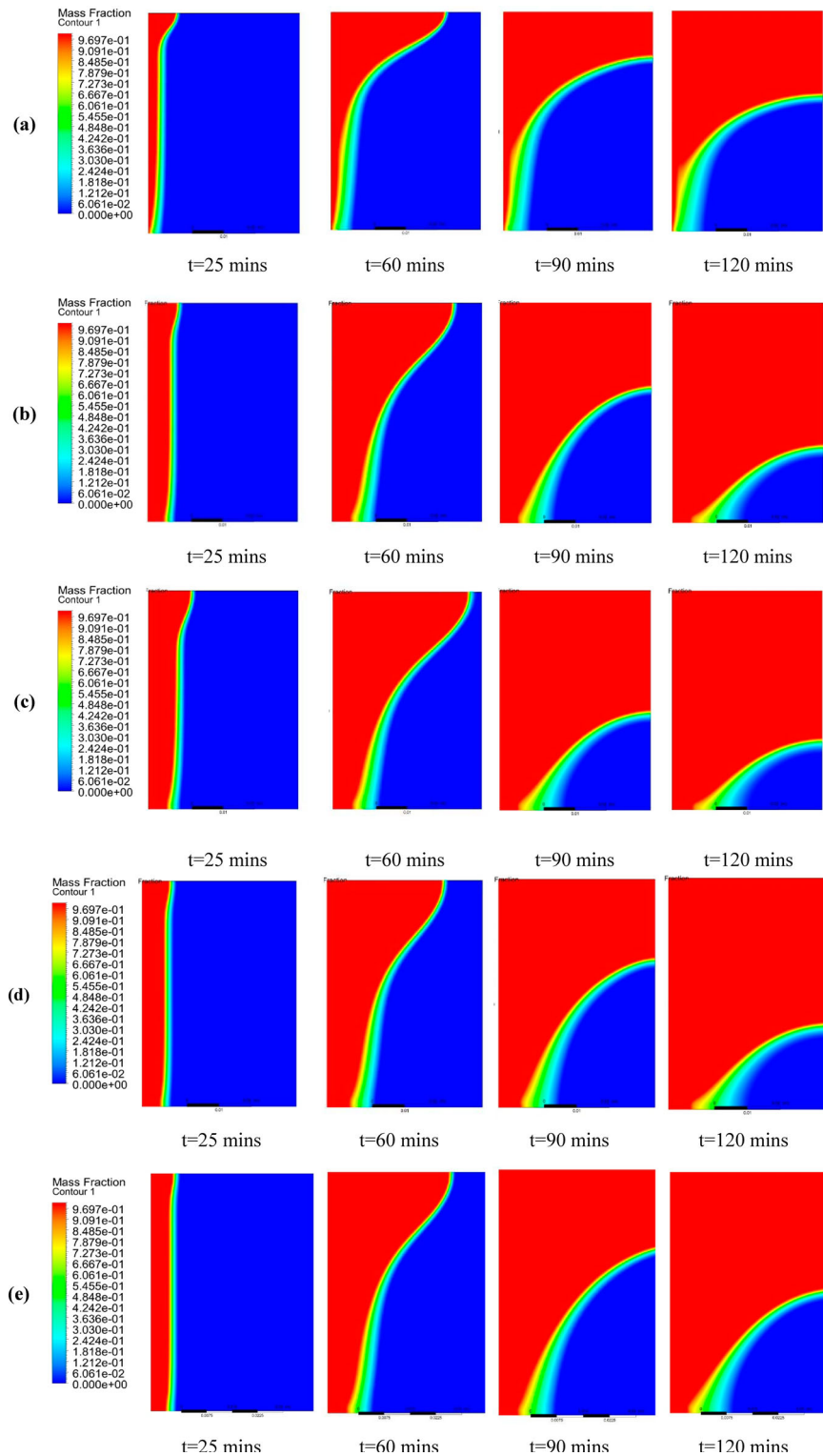
**Figure 5.** Liquid mass fractions versus flow time of paraffin with nanoparticles having mass fractions of: (a) 0 wt%; (b) 0.5 wt%; (c) 1 wt%; (d) 1.5 wt%; and (e) 2 wt%.

directing from the bottom to the top of the chamber (Sadegh et al., 2020).

Furthermore, the addition of magnetic $Fe_3O_4$ nanoparticles has revealed positive contributions to the melting process by enhancing the heat transfer (increasing the thermal conductivity) and consequently liquefying greater volumes of solid paraffin for the same time durations. Bearing in mind energy conservation principles, the heat transfer to the chamber takes place through three distinct means: the liquid phase's specific heat, the
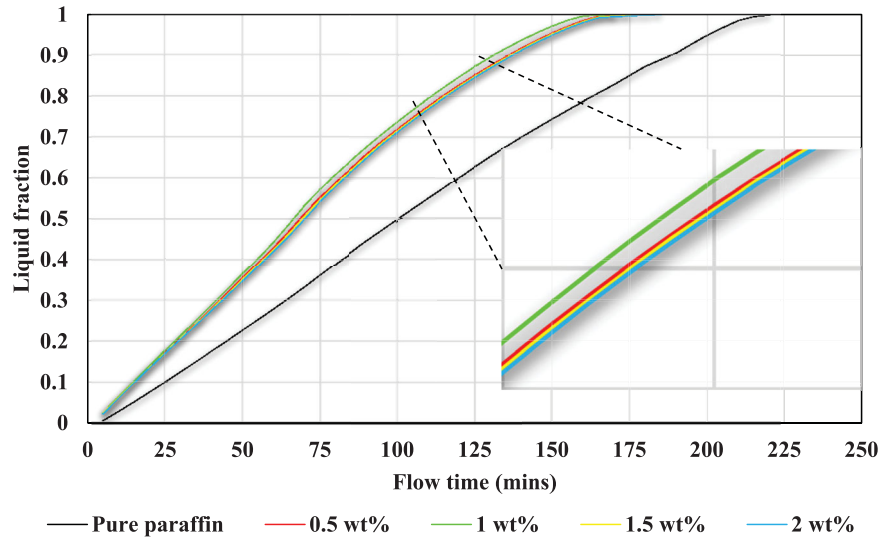
**Figure 6.** Liquid mass fractions versus flow time of pure paraffin and paraffin with nanoparticles having different mass fractions.

solid phase's specific heat and the melting latent heat. It must be noted that the effectiveness of the proposed technique lies in one important requirement, i.e. having the major volume of the imposed heat saved as latent heat. In other words, the less heat spent on raising the temperature of the solid and liquid phases, the better the PCM performs.

Moreover, as can be seen from Figure 6, the 1 wt% nanoparticle case study was more beneficial, as it led to more solid paraffin being melted. On the other hand, the increase in the concentration of nanoparticles causes the viscosity of the liquid zone to be increased (Águila et al., 2018; Ghalandari et al., 2019). The main negative side of such an occurrence is that the liquid phase has less tendency to move upwards as a result of the buoyancy force, which leads the convective heat transfer to plummet. Thus, the natural convection of the liquid phase is weakened, resulting in a lower liquid fraction of the paraffin at a concentration of 2 wt%. In fact, the increase in nanoparticle mass fraction is advantageous as long as the enhancement of the thermal conductivity outweighs the increase in viscosity. Meanwhile, as a consequence of that mass fraction, the heat transfer tends to decrease (Essaaidi & Zaz, 2015; Ouikhalfan et al., 2015; Ouikhalfan et al., 2019).

It must be noted that the total time required for all the pure paraffin to melt was over approximately 220 min, whereas, for the optimum nanoparticle concentration (1 wt%), this duration was improved by 25% to almost 165 min. Figure 7 exhibits the temperature distributions of pure paraffin and nanoparticle-enhanced paraffin for various concentrations of nanoparticles. Furthermore, the temperature of the solid phase is relatively higher for the optimum mass fraction case study in comparison to other cases. In the case of nanoparticle-enhanced paraffin, the enhancement of the melting process is mainly due to the enhanced thermal conductivity of the paraffin caused by the presence of magnetite nanoparticles. In other words, a greater portion of heat is transferred to melt the solid paraffin and consequently less stored heat is consumed to raise the liquid temperature; thus, the 1 wt% concentration of nanoparticles is the best scenario to be used among the tested concentrations.

Figure 8 illustrates the temperature distributions of five different points within the chamber as assumed in Figure 1. Locations are chosen as such to be appropriate representatives of critical zones. It is worth noting that the change in the slope, as highlighted, conveys the time that the melting process initiates. It is found that, as the temperature of each point meets the melting point, the temperature rises sharply, which is attibuted to the change of heat transfer mode from conduction (which is weak because of paraffin's low thermal conductivity) to convection. Also, as given by Figure 8(a), since point 2 is closer to the melting profile, the temperature rise is observed first at this point. In order to provide a deeper insight into the effect of nanoparticle concentration on temperature, the temperatures at point 2 for other tested cases are also presented in Figures 8(b) and 8(c). It is noticed that the addition of nanoparticles leads to a higher slope in temperature lines compared to pure paraffin owing to the enhanced conductivity of nanoparticle-fortified paraffin. In addition, as stated earlier, the temperature rises sharply as the temperature reaches the melting point, which is due to the introduction of convective heat transfer in addition to previously existing conduction.
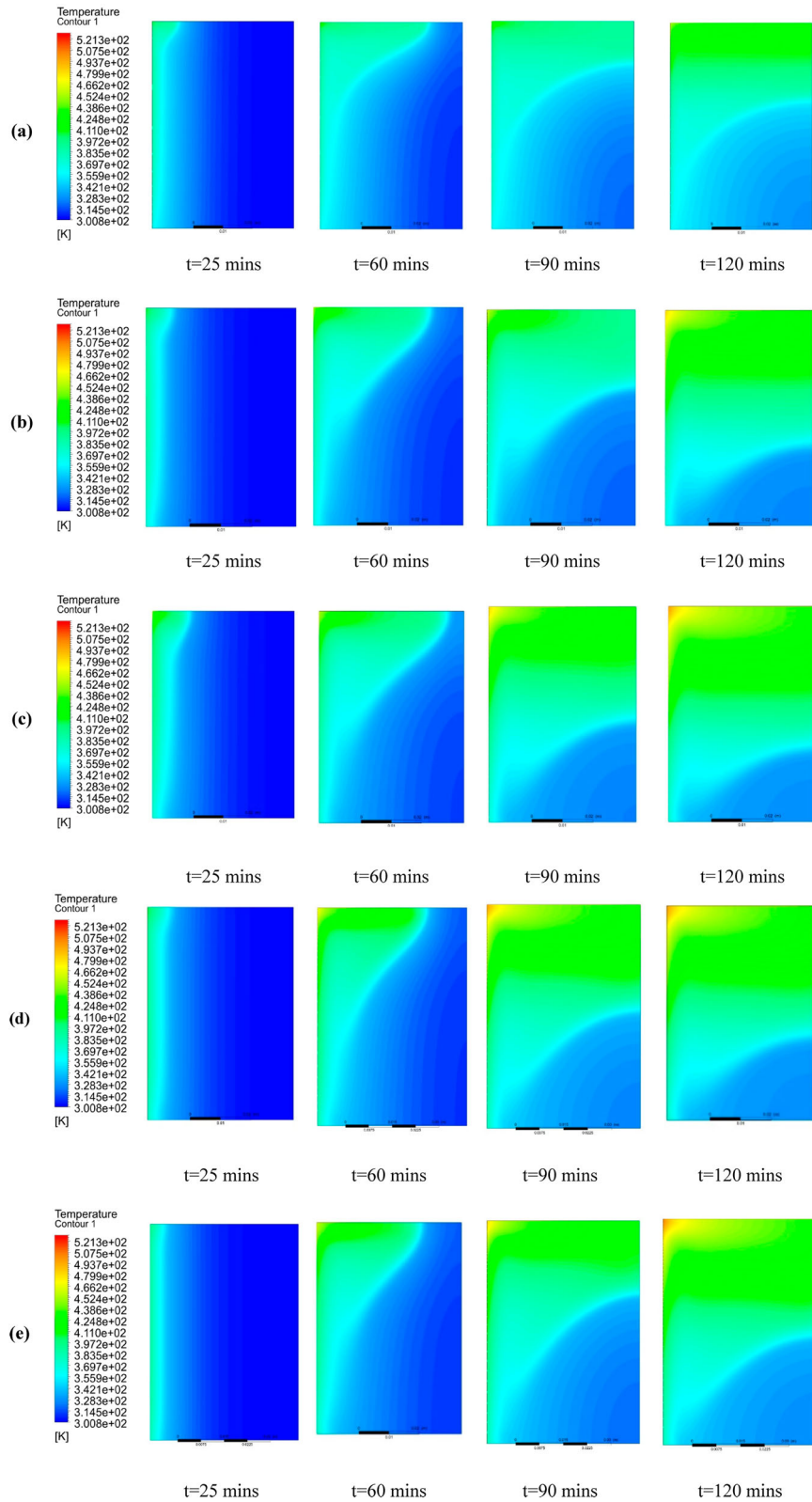
**Figure 7.** Temperature distributions versus flow time of paraffin with nanoparticles having concentrations of: (a) 0 wt%; (b) 0.5 wt%; (c) 1 wt%; (d) 1.5 wt%; and (e) 2 wt%.
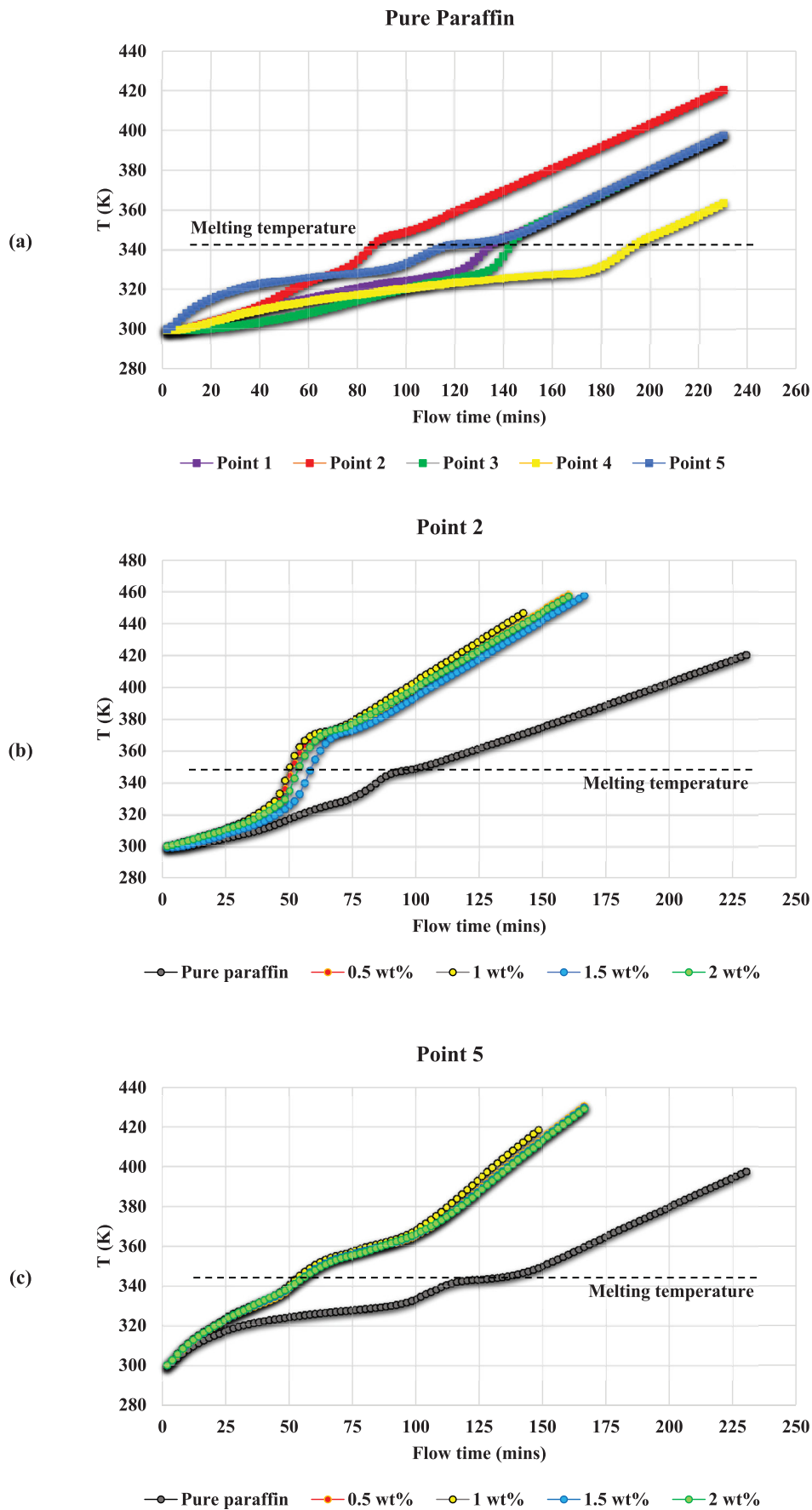
**(a)**



**(b)**



**(c)**



**Figure 8.** Temperature distribution lines for: (a) pure paraffin; and paraffin having different nanoparticle concentrations at (b) point 2; and (c) point 5.
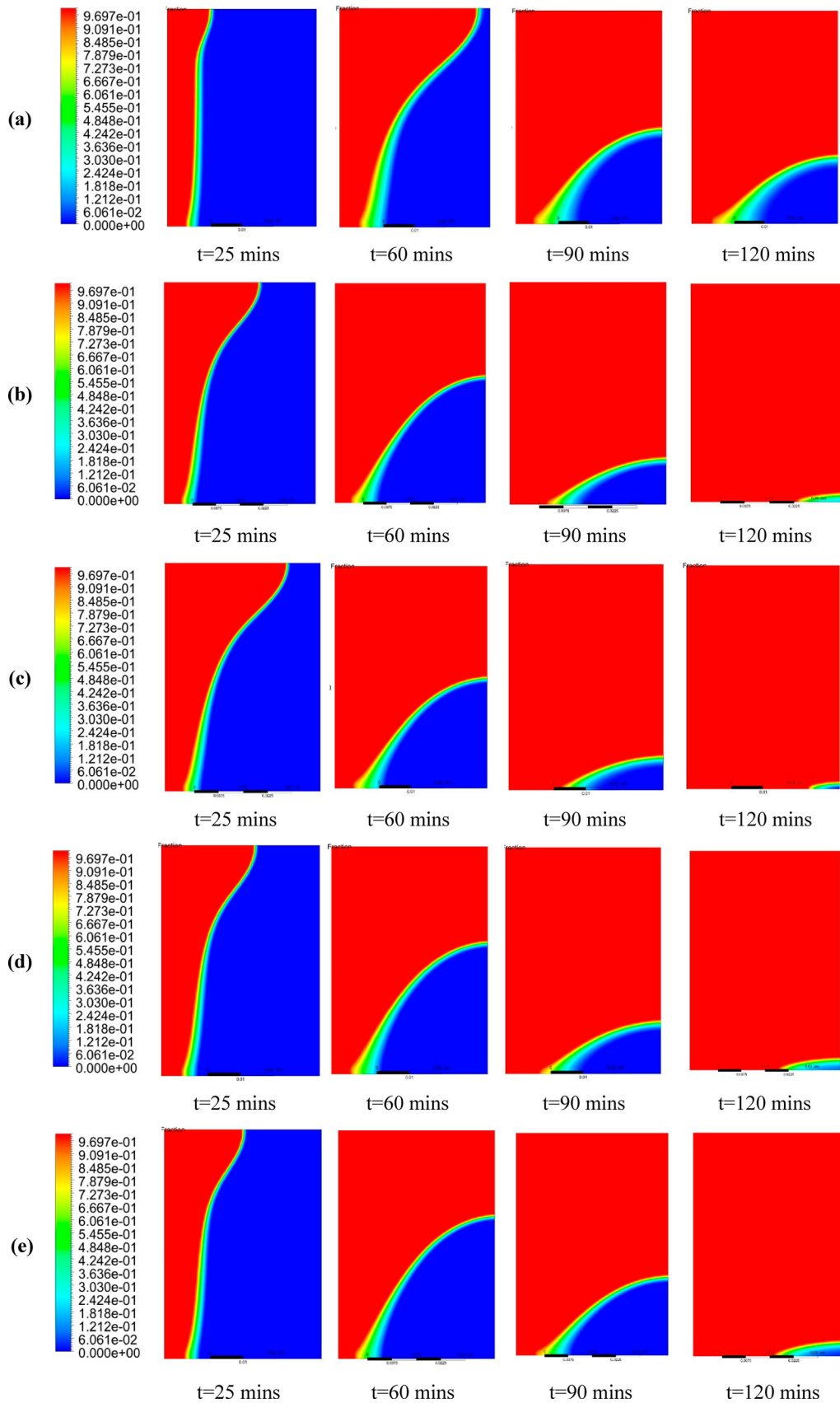
**Figure 9.** Liquid mass fractions versus flow time of 1 wt% nanoparticles at magnetic field intensities of: (a) 0 T; (b) 0.005 T; (c) 0.01 T; (d) 0.015 T; and (e) 0.02 T.
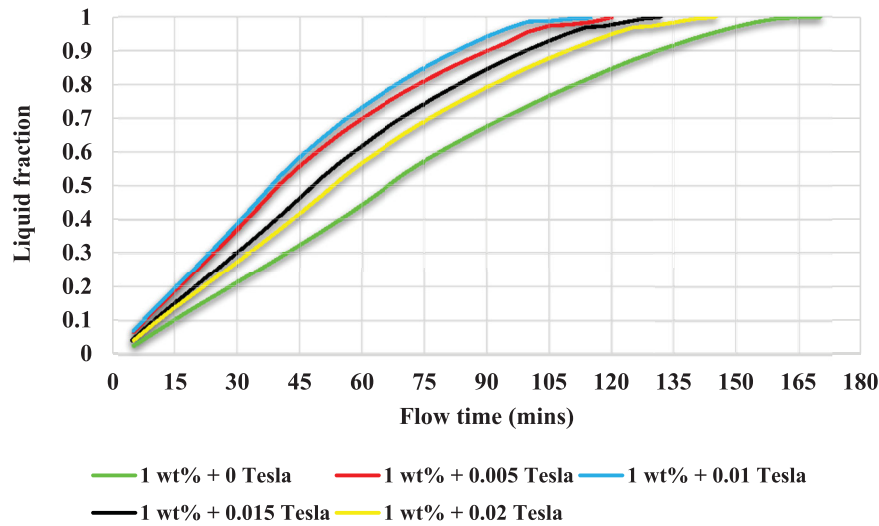
**Figure 10.** Liquid mass fractions of 1 wt% nanoparticles under various applied magnetic field intensities.

### Phase change characteristics under different magnetic fields

In this section, the contribution of applying a uniform external magnetic field at different intensities is investigated for the optimum nanoparticle mass fraction (1 wt%). In order to do this, four magnetic intensities of 0.005, 0.01, 0.015 and 0.02 T are employed, and their impacts in terms of liquid mass fractions and temperature distributions are studied. Figures 9 and 10 illustrate the liquid mass fractions for the 1 wt% nanoparticle-containing PCM under two scenarios, with and without an external magnetic field. As is revealed by Figure 9, the utilization of a magnetic field has significant outcomes, in which, for the same time duration, more solid phase is melted in all cases compared to pure paraffin. Moreover, applying a magnetic field of 0.01 T showed better heat transfer to the solid zone. In fact, the melting time for 0.01 T was enhanced by almost 24% and reduced to 125 min, in comparison to pure paraffin. In other words, using a magnetic field reduces the temperature rise of the liquid phase, particularly closer to the heater vicinity, which leads to higher transferred heat to the solid part. Furthermore, the reason behind this enhancement can be attributed to the formation of highly thermal conductive clusters of nanoparticles in the presence of a magnetic field, which lessens the difficulties associated with heat being transferred to the solid zone.

Despite the aforementioned favorable contributions of using magnetic fields, there are important issues concerning the rise in viscosity with the rise in magnetic field intensity (Gupta, 2016; Nkurikiyimfura et al., 2013). This shortcoming is due to the cluster structure as well as the horizontal magnetic force. In other words, since the clusters are structured horizontally, the shear force hinders the lighter phase from moving upwards. To shed light on this matter, it can be stated that the magnetic forces try to attract the nanoparticles towards the heater, which acts as a considerable resistance in the way of vertical displacement of the liquid phase, and consequently, leads to a decline in the natural convection of molten paraffin. Therefore, by a further increase in magnetic field intensity to 0.02 T, heat transfer reduces due to the reduction in convection. Thus, the increase in magnetic field intensity is favorable as long as the growth in viscosity does not stop the convective heat transfer. The temperature distribution profiles of 1 wt% nanoparticle-containing PCM with and without different magnetic fields are shown in Figure 11.

Figure 12 gives a comparative analysis of the temperature distribution lines for the optimum magnetite mass fraction with and without applied magnetic fields for two assumed locations. As can be inferred from the results, the utilization of a magnetic field has shown a positive improvement in the melting time. However, the 0.01 T magnetic field was superior in comparison to the other case studies tested for the reasons stated above.

### Heat transfer coefficient

To provide a concise demonstration of the heat transfer performance for the simulated cases, the average heat transfer coefficient can be used as a comparative benchmark. This feature can be formulated as follows (Karar et al., 2021; Sadegh et al., 2020):

$$\bar{h} = \frac{P}{A \times \Delta T} \tag{13}$$

where $A$, $P$ and $\Delta T$ are the heater area, applied power (which is equal to 6 W or approximately 1786 W/m$^2$)
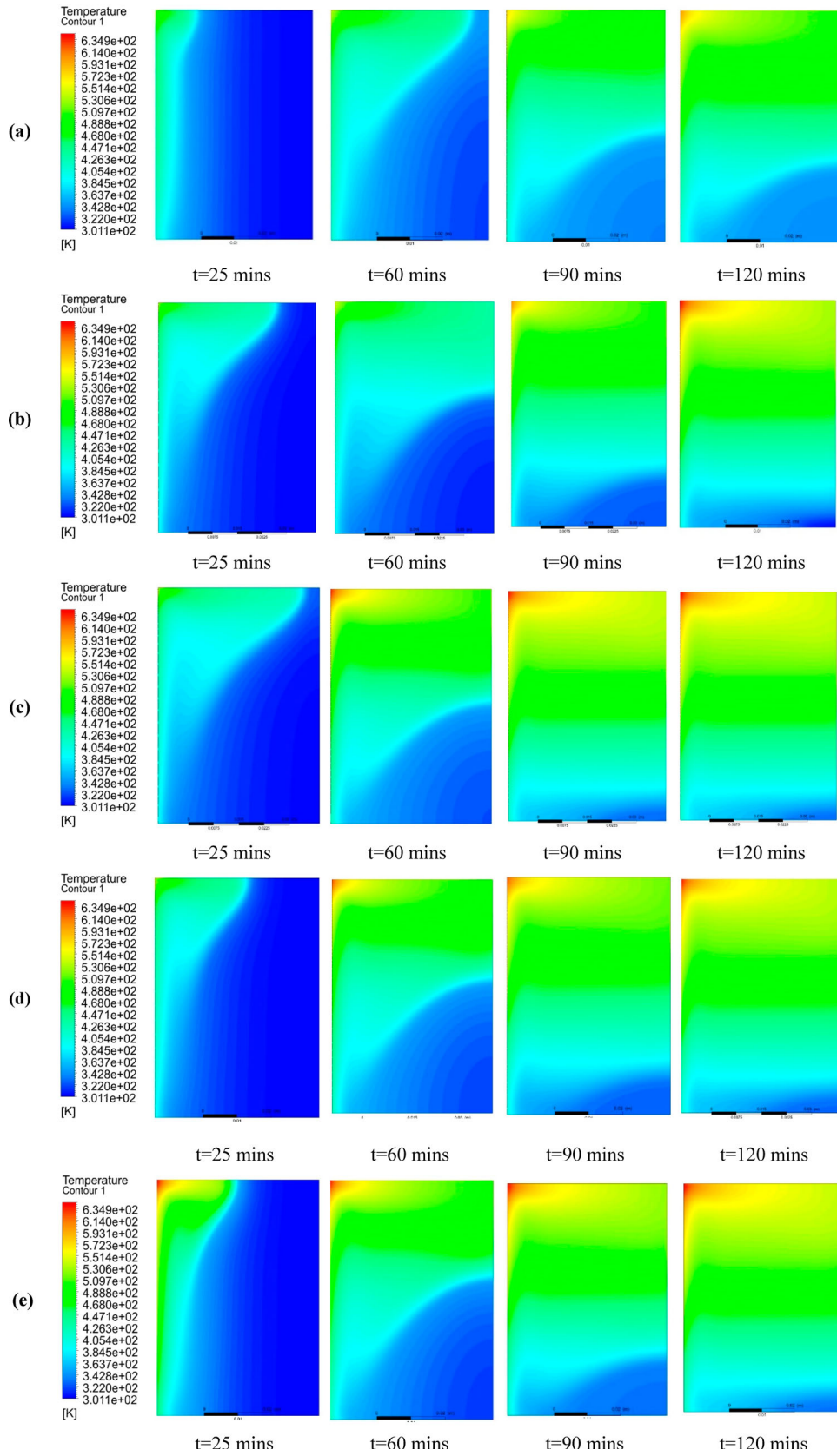
**Figure 11.** Temperature distribution profiles versus increments of time of a 1 wt% nanoparticle mass fraction at magnetic field intensities of: (a) 0 T; (b) 0.005 T; (c) 0.01 T; (d) 0.015 T; and (e) 0.02 T.
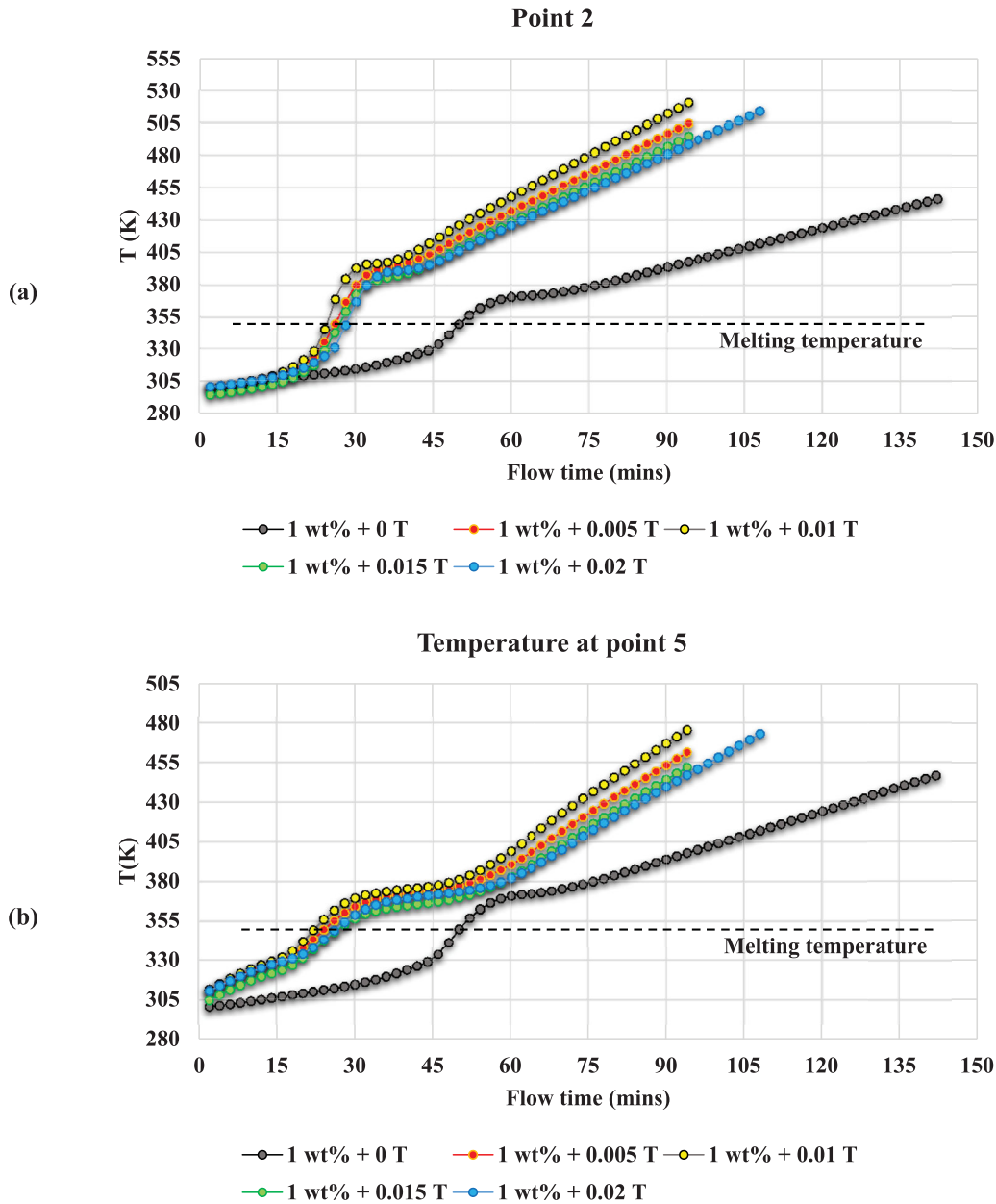
**Figure 12.** Temperature distribution lines versus flow time of a 1 wt% nanoparticle mass fraction under different magnetic field intensities at: (a) point 2; and (b) point 5.

and the temperature difference between the heater and the melting point, respectively. In order to measure $\Delta T$, numerous points throughout the left side of the chamber are considered to be representatives of the heater temperature (Sadegh et al., 2020). Afterwards, an average of the retrieved temperature is calculated and considered as the heater temperature.

According to Figure 13, it was found that convection declines with the increase in flow time. This can be attributed to the rise in heater temperature with time, which leads the $\Delta T$ term to be increased. It is ascertained

that the effective convective heat transfer values for the nanoparticle-containing PCM is higher because of the improved conductivity of paraffin. Furthermore, the application of a magnetic field contributed favorably and enhanced the convective heat transfer term. To be more exact, according to the results, the values of $h$ at $t \approx 100$ min for the optimum nanoparticle mass fraction with and without a magnetic field were approximately 138 and 121 W/m$^2$K, respectively, which were significantly (almost more than double) higher than the simulated pure paraffin (69.97 W/m$^2$K).
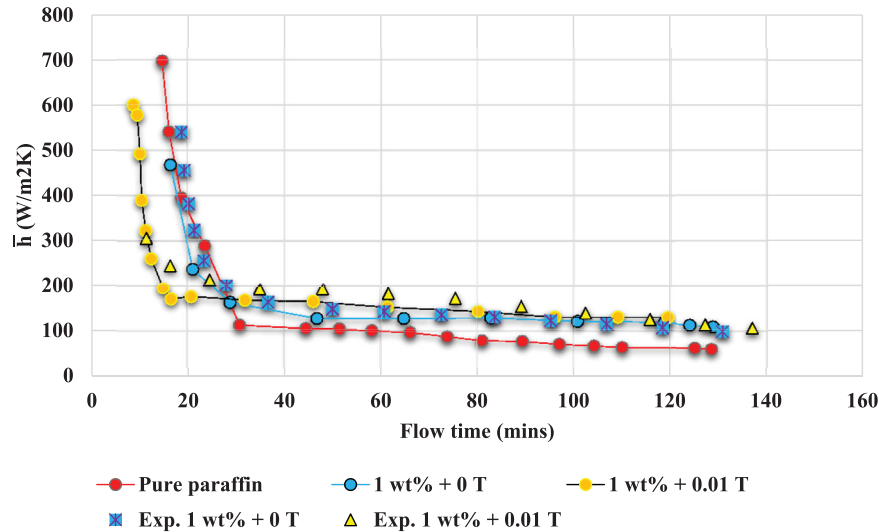
**Figure 13.** Calculated heat transfer coefficients for pure paraffin and a 1 wt% nanoparticle mass fraction at different magnetic intensities compared to experimental data (Sadegh et al., 2020).

## Conclusions

In this study, the effects of applying magnetic $Fe_3O_4$ nanoparticles with an external magnetic field to the melting process of PCM are investigated numerically. The results reveal that the incorporation of nanoparticles is not linearly proportional to the reduction in melting time or enhancement of the heat transfer coefficient. In fact, there is an optimum scenario in which the phase change characteristics perform satisfactorily. As such, among the tested case studies, the addition of 1 wt% nanoparticles revealed the best outcomes. To be exact, the melting time for 1 wt% nanoparticle-containing PCM has been improved by up to 25% compared to pure paraffin, while the melting time of 1 wt% nanoparticle-containing PCM in the presence of an external magnetic field was enhanced by up to 24% compared to no applied magnetic field. The heat transfer coefficient is also dramatically altered. As such, its value for 1 wt% nanoparticles both with and without an external magnetic field was nearly doubled compared to the pure paraffin case. Additionally, the results were also in good agreement with experimental data.

Moreover, the magnetic field in this study was applied only from one side of the chamber, which caused the last stage of the melting to take more time since the remaining solid section was trapped in the opposite corner and was hard to reach by the transferred heat. Hence, one recommendation for future work could be to use a magnetic field from several directions and sides. In particular, a movable magnetic field setup that can swirl around the chamber is preferred. Additionally, cylindrical chambers with PCM in the inner cylinder and two outer layers for the heater and magnetic field are deemed more effective if the simulation is to be conducted in 3D. However, this is subject to the optimum configuration of mushy zone constant nanoparticle concentrations as well as the external magnetic field intensity, since the melting-related phenomena are found to be profoundly affected under different values.

## Nomenclature

| | |
|---|---|
| $A$ | heater cross-sectional area (m$^2$) |
| $A_{mush}$ | mushy zone constant (kg/m$^3$s) |
| $C_p$ | specific heat capacity (J/kgK) |
| $f$ | external body force per mass unit (N/kg) |
| $f_b$ | buoyancy force (N/kg) |
| $f_m$ | magnetic force (N/kg) |
| $F_o$ | Fourier number |
| $g$ | gravitational acceleration (m/s$^2$) |
| $h$ | heat transfer coefficient (W/m$^2$K) |
| $H$ | total enthalpy (J/kg) |
| $k$ | thermal conductivity (W/mK) |
| $l$ | characteristic length (m) |
| $L$ | latent heat of melting (J/kg) |
| $m_0$ | nanoparticle bulk magnetism |
| $\nabla M$ | magnetic intensity gradient (T/m) |
| $p$ | pressure (Pa) |
| $P$ | applied power (W) |
| Pr | Prandtl number |
| $\dot{q}$ | latent heat source term (J/m$^3$s) |
| Ra | Rayleigh number |
| St | Stefan number |
| $t$ | time (s) |
| $T$ | temperature (K) |
| $T_h$ | high temperature (K) |

| | |
|---|---|
| $T_c$ | cold temperature (K) |
| $u$ | velocity vector (m/s) |
| $u_0$ | vacuum permeability (s/m-e$^2$) |
| $X$ | melt height (m) |

### Greek symbols

| | |
|---|---|
| $\alpha$ | thermal diffusivity (m$^2$/s) |
| $\beta$ | thermal expansion (K$^{-1}$) |
| $\mu$ | dynamic viscosity (kg/m-s) |
| $\rho$ | density (kg/m$^3$) |
| $\nu$ | kinematic viscosity (m$^2$/s) |
| $\gamma$ | liquid fraction |

### Subscriptions

| | |
|---|---|
| $c$ | cold wall |
| $h$ | hot wall |
| $ref$ | reference value |
| $m$ | magnetic |
| $b$ | buoyancy |

### Abbreviations

| | |
|---|---|
| wt | by mass |
| PCM | phase change material |
| TES | thermal energy storage |
| MHD | magnetohydrodynamics |
| VOF | volume of fluid method |

## Disclosure statement

No potential conflict of interest was reported by the authors.

## ORCID

*Mohammad Hossein Ahmadi*   http://orcid.org/0000-0002-0097-2534

## References

Aghaei, A., Bhattacharyya, S., Dezfulizadeh, A., Goldanlou, A., Rostami, S., & Sharifpur, M. (2021). Heat transfer and fluid flow analysis using nanofluids in diamond-shaped cavities with novel obstacles. *Engineering Applications of Computational Fluid Mechanics*, *15*(1), 1034–1056. https://doi.org/10.1080/19942060.2021.1930170

Águila, B., Vasco, D. A., Galvez, P., & Zapata, P. A. (2018). Effect of temperature and CuO-nanoparticle concentration on the thermal conductivity and viscosity of an organic phase-change material. *International Journal of Heat and Mass Transfer*, *120*, 1009–1019. https://doi.org/10.1016/j.ijheatmasstransfer.2017.12.106

Ahmed, N., Elfeky, K., Lu, L., & Wang, Q. (2019). Thermal and economic evaluation of thermocline combined sensible-latent heat thermal energy storage system for medium temperature applications. *Energy Conversion and Management*, *189*, 14–23. https://doi.org/10.1016/j.enconman.2019.03.040

Arıcı, M., Tütüncü, E., Kan, M., & Karabay, H. (2017). Melting of nanoparticle-enhanced paraffin wax in a rectangular enclosure with partially active walls. *International Journal of Heat and Mass Transfer*, *104*, 7–17. https://doi.org/10.1016/j.ijheatmasstransfer.2016.08.017

Baghban, A., Jalali, A., Shafiee, M., Ahmadi, M. H., & Chau, K.-w. (2019). Developing an ANFIS-based swarm concept model for estimating the relative viscosity of nanofluids. *Engineering Applications of Computational Fluid Mechanics*, *13*(1), 26–39. https://doi.org/10.1080/19942060.2018.1542345

Bahiraei, M., & Hangi, M. (2015). Flow and heat transfer characteristics of magnetic nanofluids: A review. *Journal of Magnetism and Magnetic Materials*, *374*, 125–138. https://doi.org/10.1016/j.jmmm.2014.08.004

Band, S. S., Bateni, S. M., Almazroui, M., Sajjadi, S., Chau, K.-w., & Mosavi, A. (2021). Evaluating the potential of offshore wind energy in the gulf of Oman using the MENA-CORDEX wind speed data simulations. *Engineering Applications of Computational Fluid Mechanics*, *15*(1), 613–626. https://doi.org/10.1080/19942060.2021.1893225

Chiew, J., Chin, C., Toh, W., Gao, Z., & Jia, J. (2018). Low-temperature macro-encapsulated phase change material based thermal energy storage system without air void space design. *Applied Thermal Engineering*, *141*, 928–938. https://doi.org/10.1016/j.applthermaleng.2018.06.060

Chiew, J., Chin, C., Toh, W., Gao, Z., & Jia, J. (2019). Thermal state-of-expansion or melting of phase change material based heat sink for underwater battery power system. *Journal of Energy Storage*, *26*, 100956. https://doi.org/10.1016/j.est.2019.100956

Dhaidan, N. S., & Khodadadi, J. (2017). Improved performance of latent heat energy storage systems utilizing high thermal conductivity fins: A review. *Journal of Renewable and Sustainable Energy*, *9*(3), 034103. https://doi.org/10.1063/1.4989738

Essaaidi, M., & Zaz, Y. (2015). *Proceedings of 2015 IEEE International Renewable and Sustainable Energy Conference:(IRSEC'15)*. IEEE.

Fluent, A. (2019). *R2 user's guide*. ANSYS Inc.

Ghachem, K., Selimefendigil, F., Öztop, H. F., Almeshaal, M., Alhadri, M., & Kolsi, L. (2021). Effects of magnetic field, binary particle loading and rotational conic surface on phase change process in a PCM filled cylinder. *Case Studies in Thermal Engineering* 28, 101456. https://doi.org/10.1016/j.csite.2021.101456

Ghadbeigi, L., Day, B., Lundgren, K., & Sparks, T. D. (2018). Cold temperature performance of phase change material based battery thermal management systems. *Energy Reports*, *4*, 303–307. https://doi.org/10.1016/j.egyr.2018.04.001

Ghalandari, M., Mirzadeh Koohshahi, E., Mohamadian, F., Shamshirband, S., & Chau, K. W. (2019). Numerical simulation of nanofluid flow inside a root canal. *Engineering Applications of Computational Fluid Mechanics*, *13*(1), 254–264. https://doi.org/10.1080/19942060.2019.1578696

Ghoghaei, M. S., Mahmoudian, A., Mohammadi, O., Shafii, M. B., Jafari Mosleh, H., Zandieh, M., & Ahmadi, M. H. (2020). A review on the applications of micro-/nano-encapsulated phase change material slurry in heat transfer and thermal

storage systems. *Journal of Thermal Analysis and Calorimetry*, 1–24. https://doi.org/10.1007/s10973-020-09697-6

Gupta, M. (2016). A review on the improvement in convective heat transfer properties using magnetic nanofluids. *Int. J. Therm. Technol*, 6(1), 40–46.

Hameter, M., & Walter, H. (2016). Influence of the mushy zone constant on the numerical simulation of the melting and solidification process of phase change materials. *Computer Aided Chemical Engineering*, Vol. 38, 439–444. Elsevier. https://doi.org/10.1016/B978-0-444-63428-3.50078-3

Hosseininaveh, H., Mohammadi, O., Faghiri, S., & Shafii, M. B. (2021). A comprehensive study on the complete charging-discharging cycle of a phase change material using intermediate boiling fluid to control energy flow. *Journal of Energy Storage*, 35, 102235. https://doi.org/10.1016/j.est.2021.102235

Hu, Y., Shi, L., Zhang, Z., He, Y., & Zhu, J. (2020). Magnetic regulating the phase change process of Fe3O4-paraffin wax nanocomposites in a square cavity. *Energy Conversion and Management*, 213, 112829. https://doi.org/10.1016/j.enconman.2020.112829

Huang, R., Li, Z., Hong, W., Wu, Q., & Yu, X. (2019). Experimental and numerical study of PCM thermophysical parameters on lithium-ion battery thermal management. *Energy Reports*.

Karar, O., Emani, S., Marappa Gounder, R., Myo Thant, M. M., Mukhtar, H., Sharifpur, M., & Sadeghzadeh, M. (2021). Experimental and numerical investigation on convective heat transfer in actively heated bundle-pipe. *Engineering Applications of Computational Fluid Mechanics*, 15(1), 848–864. https://doi.org/10.1080/19942060.2021.1920466

Kheirabadi, A. C., & Groulx, D. (2015). The effect of the mushy-zone constant on simulated phase change heat transfer. (Ed.), (Eds.). Proceedings of CHT-15. 6 th International Symposium on ADVANCES IN COMPUTATIONAL HEAT TRANSFER.

Khorampoor, N., Farahani, S. D., & Mosavi, A. (2020). Modeling the efficiency and emissions of a hybrid solar-gas power plant. *Engineering Applications of Computational Fluid Mechanics*, 14(1), 790–804. https://doi.org/10.1080/19942060.2020.1778091

Kibria, M., Anisur, M., Mahfuz, M., Saidur, R., & Metselaar, I. (2015). A review on thermophysical properties of nanoparticle dispersed phase change materials. *Energy Conversion and Management*, 95, 69–89. https://doi.org/10.1016/j.enconman.2015.02.028

Kumar, M., & Krishna, D. J. (2017). Influence of mushy zone constant on thermohydraulics of a PCM. *Energy Procedia*, 109, 314–321. https://doi.org/10.1016/j.egypro.2017.03.074

Kyriaki, E., Konstantinidou, C., Giama, E., & Papadopoulos, A. M. (2018). Life cycle analysis (LCA) and life cycle cost analysis (LCCA) of phase change materials (PCM) for thermal applications: A review. *International Journal of Energy Research*, 42(9), 3068–3077. https://doi.org/10.1002/er.3945

Lashgari, S., Mahdavian, A. R., Arabi, H., Ambrogi, V., & Marturano, V. (2018). Preparation of acrylic PCM microcapsules with dual responsivity to temperature and magnetic field changes. *European Polymer Journal*, 101, 18–28. https://doi.org/10.1016/j.eurpolymj.2018.02.011

Li, H., Wang, L., He, Y., Hu, Y., Zhu, J., & Jiang, B. (2015). Experimental investigation of thermal conductivity and viscosity of ethylene glycol based ZnO nanofluids. *Applied Thermal Engineering*, 88, 363–368. https://doi.org/10.1016/j.applthermaleng.2014.10.071

Liu, L., Su, D., Tang, Y., & Fang, G. (2016). Thermal conductivity enhancement of phase change materials for thermal energy storage: A review. *Renewable and Sustainable Energy Reviews*, 62, 305–317. https://doi.org/10.1016/j.rser.2016.04.057

Luo, K., Yao, F.-J., Yi, H.-L., & Tan, H.-P. (2015). Lattice boltzmann simulation of convection melting in complex heat storage systems filled with phase change materials. *Applied Thermal Engineering*, 86, 238–250. https://doi.org/10.1016/j.applthermaleng.2015.04.059

Marri, G. K., & Balaji, C. (2022). Liquid crystal thermography based study on melting dynamics and the effect of mushy zone constant in numerical modeling of melting of a phase change material. *International Journal of Thermal Sciences*, 171, 107176. https://doi.org/10.1016/j.ijthermalsci.2021.107176

Martin, V., He, B., & Setterwall, F. (2010). Direct contact PCM–water cold storage. *Applied Energy*, 87(8), 2652–2659. https://doi.org/10.1016/j.apenergy.2010.01.005

Mohammadi, O., Shafii, M. B., Rezaee Shirin-Abadi, A., Heydarian, R., & Ahmadi, M. H. (2021). The impacts of utilizing nano-encapsulated PCM along with RGO nanosheets in a pulsating heat pipe, a comparative study. *International Journal of Energy Research*, 45(13), 19481–19499. https://doi.org/10.1002/er.7056

Nkurikiyimfura, I., Wang, Y., & Pan, Z. (2013). Heat transfer enhancement by magnetic nanofluids—a review. *Renewable and Sustainable Energy Reviews*, 21, 548–561. https://doi.org/10.1016/j.rser.2012.12.039

Nourani, M., Hamdami, N., Keramat, J., Moheb, A., & Shahedi, M. (2016). Thermal behavior of paraffin-nano-Al2O3 stabilized by sodium stearoyl lactylate as a stable phase change material with high thermal conductivity. *Renewable Energy*, 88, 474–482. https://doi.org/10.1016/j.renene.2015.11.043

Ouikhalfan, M., Benmhamed, H., Chehouani, H., & Benhamou, B. (2015). Thermophysical investigation of a TiO2 embedded phase change material. (Ed.), (Eds.). 2015 3rd International Renewable and Sustainable Energy Conference (IRSEC).

Ouikhalfan, M., Sari, A., Chehouani, H., Benhamou, B., & Biçer, A. (2019). Preparation and characterization of nano-enhanced myristic acid using metal oxide nanoparticles for thermal energy storage. *International Journal of Energy Research*, 43(14), 8592–8607. https://doi.org/10.1002/er.4856

Park, S., Lee, Y., Kim, Y. S., Lee, H. M., Kim, J. H., Cheong, I. W., & Koh, W.-G. (2014). Magnetic nanoparticle-embedded PCM nanocapsules based on paraffin core and polyurea shell. *Colloids and Surfaces A: Physicochemical and Engineering Aspects*, 450, 46–51. https://doi.org/10.1016/j.colsurfa.2014.03.005

Qi, L., Zhang, Q., Niu, S., Chen, R., & Li, Y. (2021). Influencing mechanism of an external magnetic field on fluid flow, heat transfer and microstructure in aluminum resistance spot welding. *Engineering Applications of Computational Fluid Mechanics*, 15(1), 985–1001. https://doi.org/10.1080/19942060.2021.1938684

Ramazani, H. Z., Mohammadi, O., Rahgozar, I., Shafii, M. B., & Ahmadi, M. H. (2020). Super-fast discharge of phase change materials by using an intermediate boiling fluid.

*International Communications in Heat and Mass Transfer*, 115, 104597. https://doi.org/10.1016/j.icheatmasstransfer.2020.104597

Rao, Z., Wang, S., Wu, M., Lin, Z., & Li, F. (2013). Experimental investigation on thermal management of electric vehicle battery with heat pipe. *Energy Conversion and Management*, 65, 92–97. https://doi.org/10.1016/j.enconman.2012.08.014

Romanchenko, D., Kensby, J., Odenberger, M., & Johnsson, F. (2018). Thermal energy storage in district heating: Centralised storage vs. Storage in thermal inertia of buildings. *Energy Conversion and Management*, 162, 26–38. https://doi.org/10.1016/j.enconman.2018.01.068

Rösler, F., & Brüggemann, D. (2011). Shell-and-tube type latent heat thermal energy storage: Numerical analysis and comparison with experiments. *Heat and Mass Transfer*, 47(8), 1027–1033. https://doi.org/10.1007/s00231-011-0866-9

Sadegh, S. S., Aghababaei, A., Mohammadi, O., Mosleh, H. J., Shafii, M. B., & Ahmadi, M. H. (2020). An experimental investigation into the melting of phase change material using Fe 3 O 4 magnetic nanoparticles under magnetic field. *Journal of Thermal Analysis and Calorimetry*, 1–12. https://doi.org/10.1007/s10973-020-09958-4

Sathiyamoorthy, M., & Chamkha, A. (2010). Effect of magnetic field on natural convection flow in a liquid gallium filled square cavity for linearly heated side wall (s). *International Journal of Thermal Sciences*, 49(9), 1856–1865. https://doi.org/10.1016/j.ijthermalsci.2010.04.014

Selimefendigil, F., & Chamkha, A. J. (2016). Magnetohydrodynamics mixed convection in a lid-driven cavity having a corrugated bottom wall and filled with a non-newtonian power-law fluid under the influence of an inclined magnetic field. *Journal of Thermal Science and Engineering Applications*, 8(2). https://doi.org/10.1115/1.4032760

Selimefendigil, F., & Öztop, H. F. (2020). Impacts of magnetic field and hybrid nanoparticles in the heat transfer fluid on the thermal performance of phase change material installed energy storage system and predictive modeling with artificial neural networks. *Journal of Energy Storage*, 32, 101793. https://doi.org/10.1016/j.est.2020.101793

Selimefendigil, F., Oztop, H. F., & Chamkha, A. J. (2019). Natural convection in a CuO–water nanofluid filled cavity under the effect of an inclined magnetic field and phase change material (PCM) attached to its vertical wall. *Journal of Thermal Analysis and Calorimetry*, 135(2), 1577–1594. https://doi.org/10.1007/s10973-018-7714-9

Sharma, R., Ganesan, P., Tyagi, V., Metselaar, H., & Sandaran, S. (2016). Thermal properties and heat storage analysis of palmitic acid-TiO2 composite as nano-enhanced organic phase change material (NEOPCM). *Applied Thermal Engineering*, 99, 1254–1262. https://doi.org/10.1016/j.applthermaleng.2016.01.130

Sheikholeslami, M., & Mahian, O. (2019). Enhancement of PCM solidification using inorganic nanoparticles and an external magnetic field with application in energy storage systems. *Journal of Cleaner Production*, 215, 963–977. https://doi.org/10.1016/j.jclepro.2019.01.122

Sheikholeslami, M., & Rokni, H. B. (2017). Melting heat transfer influence on nanofluid flow inside a cavity in existence of magnetic field. *International Journal of Heat and Mass Transfer*, 114, 517–526. https://doi.org/10.1016/j.ijheatmasstransfer.2017.06.092

Sundar, L. S., Singh, M. K., & Sousa, A. C. (2013). Investigation of thermal conductivity and viscosity of Fe3O4 nanofluid for heat transfer applications. *International Communications in Heat and Mass Transfer*, 44, 7–14. https://doi.org/10.1016/j.icheatmasstransfer.2013.02.014

Turner, J. S. (1979). *Buoyancy effects in fluids*. Cambridge university press.

Yang, B., Bai, F., Wang, Y., & Wang, Z. (2020). How mushy zone evolves and affects the thermal behaviours in latent heat storage and recovery: A numerical study. *International Journal of Energy Research*, 44(6), 4279–4297. https://doi.org/10.1002/er.5191

Yoon, Y., Hyeon, S., Kim, D. R., & Lee, K.-S. (2018). Minimizing thermal interference effects of multiple heat sources for effective cooling of power conversion electronics. *Energy Conversion and Management*, 174, 218–226. https://doi.org/10.1016/j.enconman.2018.08.047

Zandie, M., Kazemi, A., Ahmadi, M., & Moraveji, M. K. (2021). A CFD investigation into the enhancement of down-hole de-oiling hydro cyclone performance. *Journal of Petroleum Science and Technology*, 199, 108352. https://doi.org/10.1016/j.petrol.2021.108352